



Analysis of tidal currents in the North Sea from shipboard acoustic Doppler current profiler data

Håvard Vindenes^{a,b,*}, Kjell Arild Orvik^a, Henrik Søiland^b, Henning Wehde^b

^a The Geophysical Institute, University of Bergen, Bergen, Norway

^b Institute of Marine Research, Bergen, Norway

ABSTRACT

North Sea tidal currents are determined by applying harmonic analysis to ship-borne acoustic Doppler current profiler data recorded from 1999 to 2016, covering large areas of the northern North Sea. Direct current measurement data sets of this magnitude are rare in the otherwise well investigated North Sea, and thus it is a valuable asset in studying and expanding our understanding of its tidal currents and circulation in general. The harmonic analysis is applied to a least squares fit of the current observations at a set of knot points. Results from the harmonic analysis compare favorably to tidal parameters estimated from observations from moored instruments. The analysis shows that the tides are characterized by strong semi-diurnal component, with amplitudes of the principal Lunar constituent ranging from 1.6 cm/s in the Skagerrak to 67 cm/s in the Fair Isle Channel. Diurnal tides are found to be approximately one fifth the strength of the predominant semi-diurnal constituent. Output from a regional barotropic tide model compares well to tidal current determined from the harmonic analysis of the Acoustic Doppler Current Profiler data.

1. Introduction

The North Sea is one of the most investigated marine areas in the world, however, remarkable data gaps still exist for spatial distributions and long-term records of velocity measurements (Sündermann and Pohlmann, 2011). In this study we utilize an extensive set of current measurements from ship mounted Acoustic Doppler Current Profilers (ADCPs) to estimate tidal currents for the northern North Sea. The data set, obtained from two ships of opportunity crossing the North Sea with great regularity, spans two multi-year periods between 1999 and 2016 and thus is a valuable asset in regards to extending our understanding of the circulation in the area. With this study we aim to evaluate the applicability of ship mounted ADCP data in studying tidal currents in the North Sea. To do this, we first create an overview of the tidal currents throughout much of the region, then compare the results with moored current meter data and model output.

The North Sea is a shelf sea adjacent to the North Atlantic, located between the Scandinavian peninsula, northwestern continental Europe, and Great Britain (see map in Fig. 1). It has a relatively broad connection to the North Atlantic and the Norwegian Sea at the northern edge, as well as a narrower connection to the North Atlantic through the English Channel in the south. This therefore results in an interplay of oceanic influences like tides and the North Atlantic Oscillation, and

continental influences like freshwater discharge and input of pollutants (Sündermann and Pohlmann, 2011). The North Sea is mostly shallow and rather flat, with an average depth of approximately 80 m. The Norwegian Trench, however, has the topography of a large fjord with a sill depth of around 270 m and a maximum depth in the inner end, in the Skagerrak, of approximately 700 m.

The propagation of tidal waves in the North Sea, as well as the dominant residual circulation, generally follow cyclonic patterns. The tidal wave entering from the Norwegian Sea progresses southward along the coast of Great Britain, and propagates around three amphidromic points, one off the southwestern tip of Norway, one at the eastern tip of the Dogger bank, and one near the entrance of the Southern Bight (Otto et al., 1990). Some of the Atlantic water entering along the western slope of the Norwegian Trench retroflects before reaching Skagerrak (Furnes et al., 1986), while the rest flows southward and recirculates in the Skagerrak and flows out again along the eastern slope of the trench along with water of Atlantic origin that enters the Norwegian Trench after flowing eastward from northeastern Great Britain across North Sea in what is commonly referred to as the Dooley Current (Dooley, 1974). Occasionally, an additional eastward flowing core of Atlantic Water has been observed farther north of the Dooley Current (Svendsen et al., 1991).

The bottom on the plateau west of the Norwegian Trench rises from

* Corresponding author at: Institute of Marine Research, Bergen, Norway.
E-mail address: haavard.vindenes@imr.no (H. Vindenes).

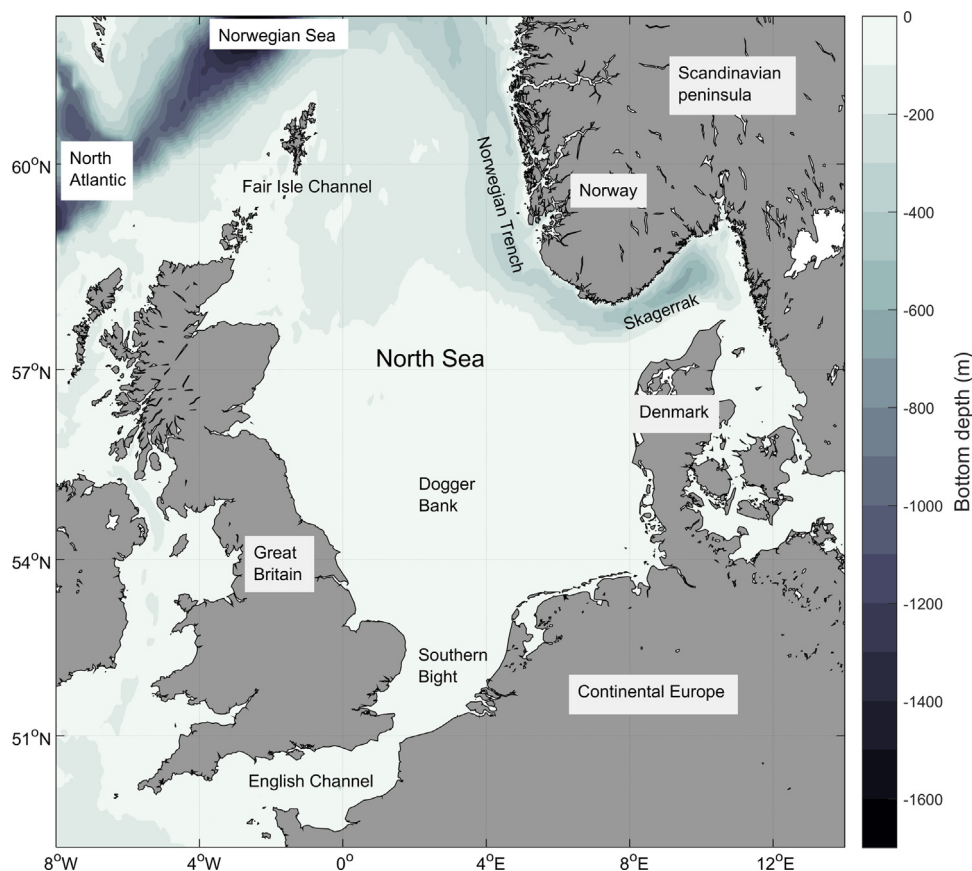


Fig. 1. A map of the North Sea and its surroundings.

a depth of 200 m at the northern edge to 20 m and less near the continental coast in the south. The topographic conditions create a divide in dynamic conditions as well, with the tidally-dominated southern and central parts, and the northern parts where the tide is less predominant. This decrease in bottom depth from north to south in the North Sea basin leads to a comparable increase in current strength (Otto et al., 1990).

Dietrich (1950) presented an illustration of maximum tidal currents for spring tides which are strongest along the coast of Great Britain and in southern parts of the North Sea where they exceed 1 m/s in some locations. Farther north maximum speeds are considerably lower, but still on the order of tens of cm/s (see Otto et al., 1990, Fig. 1.4).

Previous studies describe semidiurnal tides as the dominant harmonic components of the flow (Otto et al., 1990; Baxter et al., 2008), and that the semi-major axes of the tidal current ellipses are predominantly north-south oriented on the plateau of the central, northern North Sea, as well as in the Norwegian Trench along 59° N (Davies and Furnes, 1980; Klein et al., 1994). Tidal currents in the Skagerrak are described as weak, on the order of 1 cm/s (Rodhe, 1987; Danielssen et al., 1997), while the tidal currents in the Fair Isle Channel exceed speeds of 1 m/s (Baxter et al., 2008; Turrell et al., 1990).

The rest of this paper is organized as follows: Details about the data and the method used to extract tidal currents are given in Section 2, results are presented in Section 3 and explored further in the discussion and concluding remarks in Sections 4 and 5.

2. Data and methods

2.1. Data

The ADCP measurements used in this study have been obtained from instruments mounted on two ships of opportunity. The M/V Nuka

Arctica, a container ship which operates between Denmark and Greenland on 3-week round trips, ran a 150 kHz ADCP between 1999 and 2002, and since 2012 has been running a 75 kHz ADCP. Data from both the first and second period until late summer of 2016 are used here. The M/F Norröna, a ferry operating on a 1-week schedule between Denmark and Iceland via the Faroe Islands, is equipped with a 75 kHz ADCP. The Norröna data used here are from 2008 to 2015, excluding 2013. The ADCP tracks from the North Sea for both ships are shown in Fig. 2.

The ADCP-instruments transmit sound, commonly referred to as pings, of a known frequency along four beams down into the water column. The ping returns to the instrument with a change in frequency depending on the velocity of the ocean. If there is an oncoming current, the return frequency is increased. The combination of measurements from all four beams is combined to determine the ocean velocity in three dimensions relative to the instrument. Absolute ocean velocities are determined by subtracting the velocity of the ship. For each ping the velocity is determined and grouped in vertical bins. During processing, velocity determined from each ping are averaged over a set time increment to create ensembles. The ADCP dataset used here consists primarily of 3 min and some 5 min ensembles. The Nuka Arctica and Norröna have cruising speeds of approximately 15 knots and 20 knots, respectively, so the horizontal resolution of the ADCP data varies from around 1400–3100 m. Vertically the ADCP data are separated into 8 m bins. In the North Sea, the instruments are predominantly run in broadband mode with bottomtracking. The navigation source on both ships is the Ashtech ADU5 with a 4-antenna array.

In order to evaluate the accuracy of the extracted tidal currents from the ADCP data, current measurements from moored instruments around the North Sea have been used. Results from a number of current meters deployed during the Joint North Sea Data Project in 1976, presented by Davies and Furnes (1980) have been used (Only M_2 tide data is

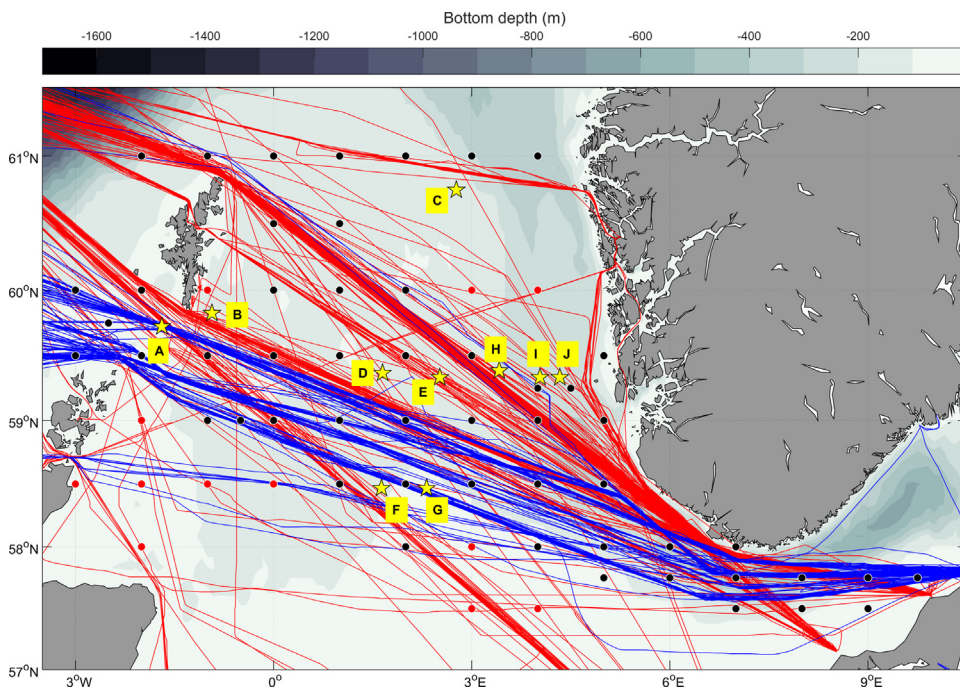


Fig. 2. Map of the northern North Sea with ADCP tracks, mooring locations, and locations of knot points used in calculation of tidal currents. Nuka Arctica and Norröna cruise tracks are marked in blue and red, respectively. The black dots mark the location of the knot points used in the tide extraction process. Red dots mark knot points with less than 150 ADCP datapoints within a surrounding circle with a radius equal to the length of 0.25 degrees of latitude. Yellow stars mark the mooring locations of the moorings listed in Table 1. (For interpretation of the references to color in this figure legend, the reader is referred to the web version of this article.)

Table 1

Mooring information. Coordinates are given in decimal degrees, and temporal resolution is given in minute averages. Any results from moorings marked with bold letters have been obtained from Davies and Furnes (1980), the actual data have not been processed here. Asterisks represent information we were not able to confirm.

Mooring	Coordinates	Deployment period	Temporal resolution	Instrument
A	59.7° N, 1.7° W	7-May-2008–27-Sep-2008	30	Aanderaa RCM-7
B	59.8° N, 0.9° W	11-May-1972–28-May-1972	60	Plessey MO21
C	60.8° N, 2.8° E	3-Feb-1979–30-Mar-1979	15	Aanderaa RCM-4
D	59.4° N, 1.7° E	10-Mar-1976–6-May-1976	10	Aanderaa RCM-4/5
E	59.3° N, 2.5° E	Mar-1976–May-1976	*	*
F	58.5° N, 1.6° E	9-Mar-1976–7-May-1976	10	Aanderaa RCM-4/5
G	58.5° N, 2.3° E	25-Mar-1976–26-Apr-1976	10	Aanderaa RCM-4/5
H	59.4° N, 3.4° E	11-May-1975–02-Jul-1975	10	Aanderaa RCM-4
I	59.3° N, 4.0° E	Mar-1976–May-1976	*	*
J	59.3° N, 4.3° E	Mar-1976–May-1976	*	*

presented in Davies and Furnes, 1980, thus that is the only constituent we are able to compare with in these particular mooring locations). Data from the Fair Isle Channel and surrounding areas were kindly provided by Marine Scotland Science (B. Berx, pers. comm. 2016), and data from the Norwegian Deep Water Programme (E. Nygaard, pers. comm. 2015) are used as well. The locations of the moorings are shown in Fig. 2. Coordinates are also listed in Table 1 along with deployment period, temporal resolution, and instrument type.

Output from a regional barotropic tide model for the northwestern European shelf with resolution of 1/30°, described by Egbert et al. (2010), is also compared with the extracted tidal currents from the ADCP measurements. The model uses Oregon State University Tidal Inversion Software (OTIS) (Egbert and Erofeeva, 2002).

Tidal ellipse parameters of current meter- and model output-time series, and the Greenwich phases of the tidal harmonics extracted from the ADCP data as well as for current meter data, have been determined using *t_tide* which is described by Pawlowicz et al. (2002).

2.2. Extracting tidal currents from the ADCP data

To analyze the tidal currents, and further utilize the ADCP dataset we work with in this study, e.g. for estimating volume transport, it is important to be able to extract the the harmonic components of the

current associated with the tide. Due to their periodic nature, the tidal currents can be separated into basic harmonic constituents. Given a sufficiently long time-series at any location the tides can be predicted with good accuracy. The longer the time series, the better the results will become, as the closely spaced constituents can be more successfully separated. In contrast to harmonic analysis of current observations from a fixed location, performing the analysis on shipborne ADCP measurements requires additional consideration of the spatial variability. To extract the tidal currents from the ADCP measurements, a detiding scheme developed by Dunn (2002) and Wang et al. (2004) has been utilized. The harmonic analysis is based on a least squares fit of the current observations that is specified at a set of knot points (the knot points utilized in our analysis are shown in Fig. 2). Here we have used 63 mainly evenly spaced knot points in a network of 0.5 degrees latitude and 1 degree longitude separation distributed around the study area. In some areas knot points have been removed or moved closer to areas with high ADCP measurement concentration. This methodology essentially allows for determination of the barotropic tide at any time at any location within the study area. The velocity components are represented by a mean current and sum of harmonic current constituents as

$$u(\mathbf{r}, t) = u_0(\mathbf{r}) + \sum_{i=1}^N [a_i(\mathbf{r})\cos(\omega_i t) + b_i(\mathbf{r})\sin(\omega_i t)], \quad (1)$$

where u_0 is the mean current field, $\mathbf{r}(x, y)$ is the position vector, a_i and b_i are amplitudes, t is time, ω_i is the frequency of a given constituent, and N is the number of constituents. Before producing the least squares fit, the ADCP data are multiplied with a Gaussian weighting function on the form

$$\phi(\mathbf{r}, \mathbf{r}_j) \sim \exp \left\{ - \left[\frac{(x - x_j)^2}{\sigma_x^2} + \frac{(y - y_j)^2}{\sigma_y^2} \right] \right\}, \quad (2)$$

where $\mathbf{r}_j(x_j, y_j)$ are the positions of the knot points and σ_x and σ_y are decay parameters controlling the shape of the Gaussian curve. In this study we mainly use an isotropic decay parameter with $\sigma_x = \sigma_y = 55.5$ km, which is equivalent to the length of half a degree of latitude. The decay parameter was chosen after experimenting with values ranging from 0.1 to 1 degree of latitude. The chosen decay parameter yielded the results that compared best with tidal parameters determined from harmonic analysis of observations from moored instruments in the North Sea (see Appendix A for a detailed discussion on the choice of decay parameter). An anisotropic decay parameter was used in only one location where we wanted to limit the zonal influence more than the meridional influence. All observations are incorporated in the calculations, with the observations closest to the knot point weighted most heavily. The decay parameter does not represent a cutoff outside of where datapoints are excluded in the calculations, however, it shapes the Gaussian curve so as to limit their influence in the determination of the tidal current at the given knot point locations.

The tidal constituents that have been extracted, six principal constituents and three overtones, are listed in Table 2 along with their respective period and frequency. Results of the extracted tidal currents from 53 m depth are presented in terms of tidal ellipse parameters in Section 3. The depth of 53 m was chosen as data is most abundant around this depth in most areas. A ship mounted ADCP is sensitive to rough seas, which especially can contaminate measurements made closer to the surface. The chosen depth is also well above the bottom depth for most non-coastal areas in the northern North Sea, thus the ADCP has a good coverage at this depth in most crossings made over our entire study area.

The ellipse parameters we have used are semi-major and semi-minor axes, ellipse inclination, and Greenwich phase lag. A simple illustration of the ellipse parameters is shown in Fig. 3. The semi-major and -minor axes represent maximum and minimum current speeds of the given tidal constituent, the inclination is the counterclockwise angle between the east direction and the semi-major axis. A negative semi-minor axis indicates a clockwise rotation of the ellipse, while a positive semi-minor axis indicates a counterclockwise rotation. Foreman (1977) illustrates the concept of the Greenwich phase lag by appointing each constituent

Table 2

Tidal constituents used in the harmonic analysis. Period is given in hours, and frequency in cycles per day.

Name of constituent	Symbol	Period	Frequency
Diurnal			
Luni-solar	K_1	23.9345	1.0027
Principal lunar	O_1	25.8193	0.9295
Semi-Diurnal			
Smaller lunar elliptic	L_2	12.1916	1.9686
Principal lunar	M_2	12.4206	1.9323
Larger lunar elliptic	N_2	12.6583	1.8960
Principal solar	S_2	12.0000	2.0000
Higher harmonics			
Shallow water overtones of principal lunar	M_4	6.2103	3.8645
	M_6	4.1402	5.7968
	M_8	3.1052	7.7291

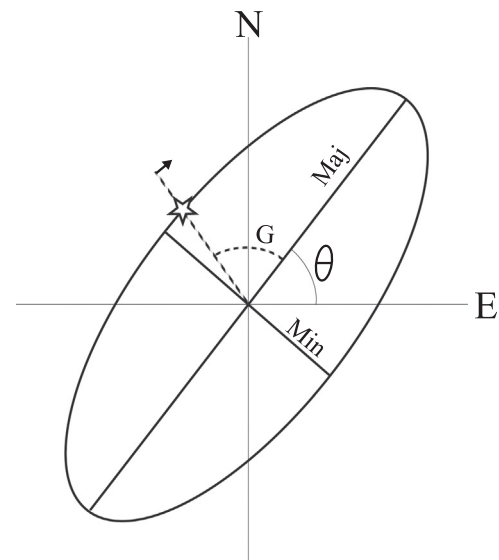


Fig. 3. Illustration of a clockwise rotating tidal current ellipse and its parameters. Maj is the Major axis and Min is the Minor axis. θ , the counterclockwise angle between East and the northern semi-major axis, is the inclination of the ellipse. The star marks where in the ellipse cycle the current is at the time of the maximum equilibrium tide at the Greenwich Meridian. G is the Greenwich phase angle which is the angular retardation between the maximum of the equilibrium tide at the Greenwich meridian and the maximum of the tidal ellipse. A detailed description of the calculation of the different ellipse parameters is given by Foreman (2004).

of the tide a fictitious star which travels around the equator with an angular speed equal to that of its corresponding constituent. The Greenwich phase lag is the angular retardation of maximum tidal current at a location behind the corresponding maximum of the equilibrium tide at the Greenwich meridian which occurs when the fictitious constituent star passes over it.

Standard deviations of tidal ellipse parameters have been calculated by bootstrapping the original ADCP measurement dataset. The original dataset is randomly resampled with replacement, such that each new dataset will have some of the original datapoints represented more than once and others not at all. The original dataset is resampled 500 times, creating 500 unique datasets of the same size. Standard deviation is then calculated from the 500 separate values calculated for each parameter after applying harmonic analysis on the resampled data.

3. Results

3.1. Harmonic analysis of the ADCP data

Fig. 4 depicts the two major semi-diurnal and the two major diurnal tidal constituents from our harmonic analysis of the ADCP data. It reveals M_2 , the principal Lunar semi-diurnal tidal constituent, as the predominant constituent. Maximum M_2 tidal current speed varies from only a few cm/s in the Skagerrak, to 67 cm/s in the Fair Isle Channel, and has an overall average maximum speed of 15.3 cm/s. The ellipses are generally elongated with the major axes oriented approximately meridionally on the plateau in the central part of our study area, between 0° and 4° East (hereinafter referred to as the plateau). In the Norwegian Trench, the ellipses are typically oriented along the trench, and as it bends around the southern tip of Norway and into the Skagerrak, they are oriented more in an east-west direction. In and around the Fair Isle Channel the ellipses are oriented along the channel. This is also where we find the strongest tidal currents, with an average maximum speed of 45.6 cm/s. Semi-major axes over the plateau vary from 8.4 cm/s to 24.9 cm/s with an average of 16.2 cm/s. The ellipses located eastward of 4° East have semi-major axes varying from 1.1 cm/s

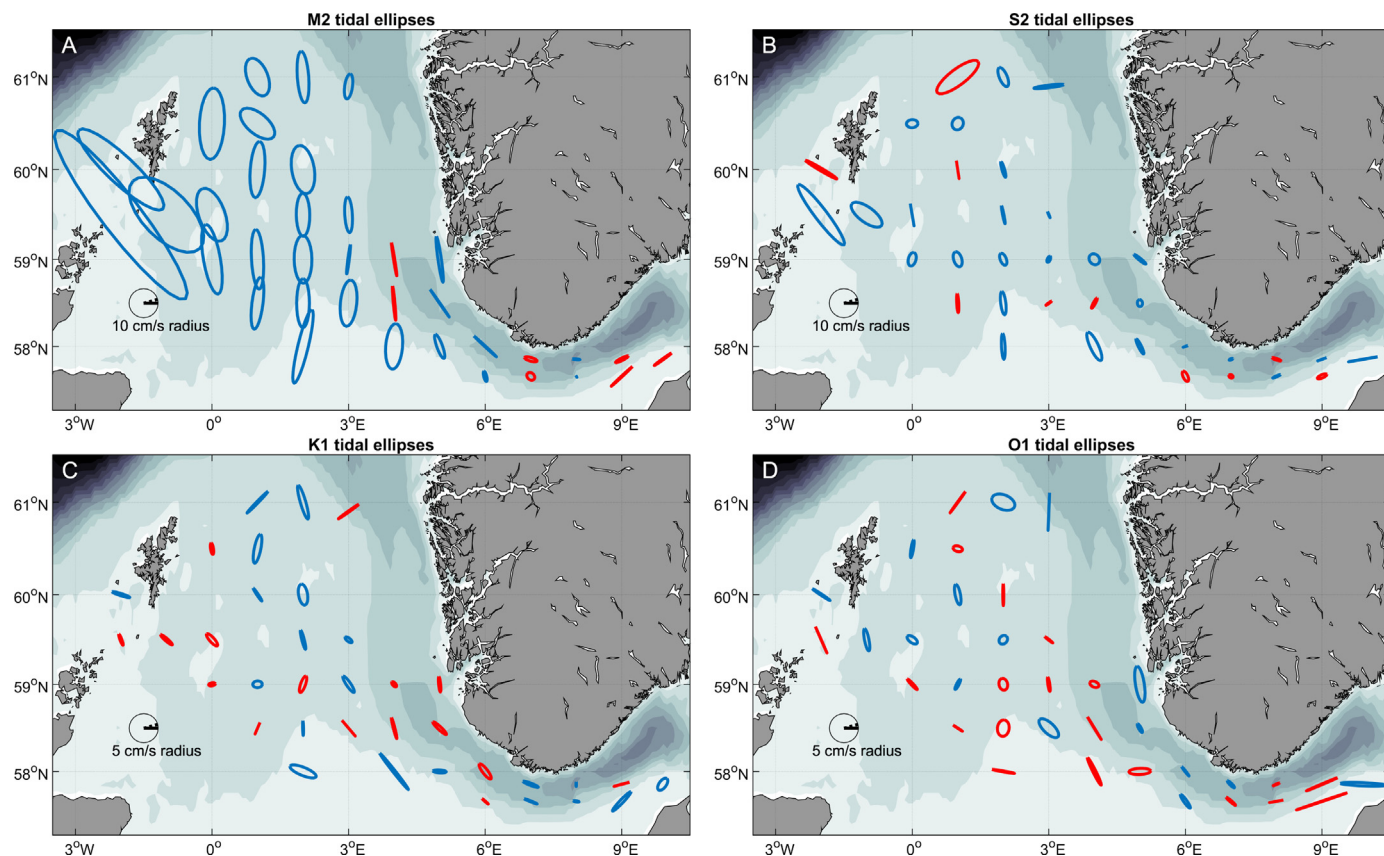


Fig. 4. Tidal ellipses of the two main semi-diurnal tidal constituents M_2 (A), and S_2 (B), and the two main diurnal tidal constituents K_1 (C), and O_1 (D). Ellipse parameters are calculated from ADCP current measurements from 53 m depth. Note that reference ellipse in (A) and (B) has a 10 cm/s radius, while in (C), and (D) it has a radius of 5 cm/s. Blue ellipses rotate clockwise, red ellipses rotate counterclockwise. (For interpretation of the references to color in this figure legend, the reader is referred to the web version of this article.)

to 16.3 cm/s with an average of 8 cm/s. In the Norwegian Trench and along the shelf near the northern coast of Denmark, the ellipses are narrow with semi-minor axes of less than 1 cm/s, revealing an essentially longitudinal tidal current. Overall, M_2 semi-minor axes are primarily negative, and most ellipses therefore rotate clockwise. The counter clockwise rotating M_2 ellipses are typically very narrow with semi-minor axes not exceeding 1 cm/s. The phase of the maximum tidal current of the M_2 in and around the Fair Isle Channel ranges from 109° to 117° , and ranges from 118° to 181° on the plateau. In the Norwegian Trench, the phase increases and varies between 173° and 219° , and even farther east in the Skagerrak the phase values range from 89° to 303° . There is a general increase of the phase values eastward, with a few exceptions at some of the southernmost ellipses on the plateau and in the Skagerrak, where the pattern is more arbitrary.

The second most prominent constituent is S_2 , the principal Solar semi-diurnal tide. Overall, the maximum S_2 tidal current speeds at the positions of the ellipses in Fig. 4 are approximately one third the speed of the maximum M_2 current speeds. Accordingly, the greatest S_2 tidal current speeds are also found in the Fair Isle Channel where they reach 24.4 cm/s. The semi-major axes of the S_2 ellipses over the plateau (excluding the northernmost ellipses) are oriented more or less meridionally, in the Skagerrak they are oriented more zonally, and in the Fair Isle Channel they are oriented along the channel. The phase of the S_2 tidal current is quite variable, revealing no clear propagating pattern compared to that we see in the phase of the M_2 tidal current. However, values on the plateau and in the Fair Isle Channel range from 110° to 279° . In the Norwegian Trench, including the Skagerrak, the phase at the different ellipse locations range from 31 to 356.

The maximum tidal current speeds of N_2 and L_2 , the larger lunar elliptic and smaller lunar elliptic constituents, are approximately one

fourth and one sixth the maximum speed of the M_2 on average.

The two main diurnal tidal constituents K_1 and O_1 both have, on average, maximum speeds that are approximately one fifth that of the M_2 . The orientation of the ellipses of the diurnal constituents is quite erratic over the plateau. In the Fair Isle Channel the diurnal ellipses are oriented similarly to the ellipses of the semi-diurnal constituents, however, we do not see the same maxima in current speeds as we do in the semi-diurnal constituents in this area. In the Skagerrak and the rest of the Norwegian Trench, the ellipses follow relatively similar inclination patterns as the M_2 ellipses which are generally oriented along the trench. On the shelf near the coast of Denmark the O_1 tidal currents reach speeds of 9 cm/s, which is slightly more than the maximum M_2 speeds at this location.

The higher harmonic tidal constituents are all relatively weak. Overall maximum current speed for M_4 , M_6 and M_8 are approximately one ninth, one twelfth, and one fifteenth the magnitude of M_2 , respectively.

3.2. Comparison with observations from moored current meters and a barotropic tide model

M_2 tidal ellipses calculated from the ADCP data, and observations from fixed current meters are presented in Fig. 5; and the parameters are presented in Table 3. The results from 10 current meters are presented here because they are located in areas of relatively high concentrations of ADCP-measurements (see Fig. 2 for ADCP cruise tracks). The semi-major axes coincide fairly well. Axes calculated from ADCP data are longer than those calculated from current meter data in 7 of 10 locations, and on average they differ by 4.4 cm/s in length. ADCP semi-minor axes are also longer in 6 of the locations, and on average they

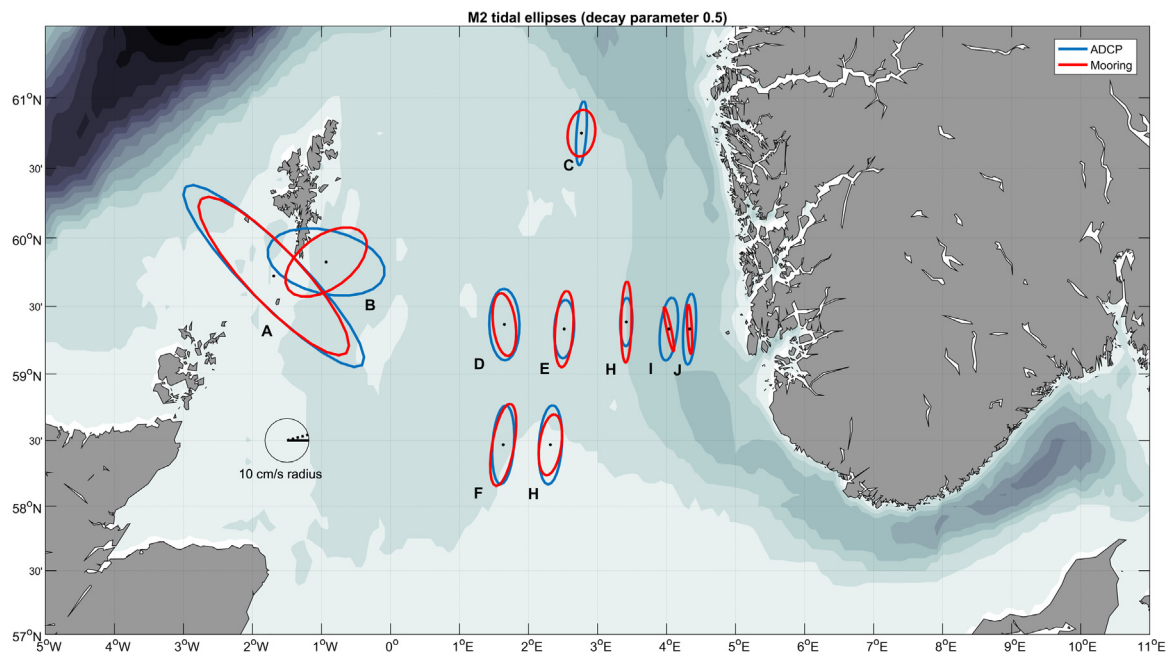


Fig. 5. M_2 tidal ellipses of extracted tidal currents from ADCP measurements at 53 m in blue compared to M_2 tidal ellipses based on data from moored current meters in red. The depth of the moored instruments are listed in Table 3. (For interpretation of the references to color in this figure legend, the reader is referred to the web version of this article.)

differ from the current meter semi-minor axes by 1.4 cm/s. All of the ellipses in Fig. 5 have negative semi-minor axes, and therefore rotate clockwise. The average deviation of the inclination is 5.3° when we exclude mooring B, where the inclination deviates by 131° .

The S_2 ellipse parameters at four of the mooring locations are presented in Table 4. S_2 semi-major axes calculated from ADCP data vary from 2.6 cm/s to 20.8 cm/s, and have a mean value of 9.8 cm/s. The harmonic analysis of the ADCP data reveals semi-major axes that are larger than current meter data in 3 of 4 locations. Only at the location of mooring H, the semi-major axis of the S_2 calculated from the data from the moored instrument is larger than the axis calculated from the ADCP data. S_2 Semi-minor axes from ADCP data vary from -5.9 cm/s to 0.2 cm/s with an average length of 3.7 cm/s, while the average length

Table 4

Same as Table 3 but for the S_2 constituent.

Mooring	Measurement depth (m)	Semi-major	Semi-minor	Inclination ($^\circ$)	Phase lag ($^\circ$ G)
A	49	15.4	-4.6	129.0	150.6
	53	20.8	-4.8	136.4	131
B	52	4.5	-2.5	18.9	273.2
	53	10.4	-5.9	148.9	120.5
C	60	3.3	-2.3	90.9	194.7
	53	5.2	-3.9	48.5	171.9
H	50	4.5	0.4	91.1	216.5
	53	2.6	0.2	84.7	174.9

Table 3

M_2 ellipse parameters calculated from moored current meters (bold text) and from the ship mounted ADCP measurements. Measurement depth is listed in m, semi-major and semi-minor axes are listed in cm/s, inclination is listed in $^\circ$ counter clockwise from east, phase lag is listed in Greenwich phase lag ($^\circ$ G), and ADCP datapoints are listed in numbers within a radius of 0.5° , and 0.25° of latitude, respectively. Standard deviations are noted in parentheses. Asterisks in the phase column mark from which moorings this information could not be obtained.

Mooring	Measurement depth (m)	Semi-major	Semi-minor	Inclination ($^\circ$)	Phase lag ($^\circ$ G)	ADCP datapoints	
						within 0.5 lat	within 0.25 lat
A	49	46.4	-11.9	133.3	112.2		
	53	54.9 (0.6)	-11.8 (0.3)	134.8 (0.4)	108.7 (0.6)	6956	1954
B	52	20.4	-11.5	36.1	234.2		
	53	26.1 (0.7)	-13.9 (0.7)	167.1 (2.8)	84.6 (2.8)	3955	781
C	60	10	-5.8	82.8	170.4		
	53	13.7 (1.0)	-2.1 (1.4)	86 (5.8)	216.8 (4.8)	447	174
D	65	14	-5	97	*		
	53	15.9 (0.5)	-6.7 (0.5)	91 (2.2)	166.26 (2.47)	5730	363
E	55	17	-4	86	*		
	53	13 (0.4)	-4.4 (0.4)	87.1 (2.3)	161.39 (2.3)	7830	1552
F	66	19	-5	80	*		
	53	18 (0.4)	-4.9 (0.3)	86.1 (1.3)	164.6 (1.1)	5827	1954
G	33	14	-5	82	*		
	53	18.1 (0.4)	-5.3 (0.5)	86.5 (1.4)	162.6 (1.4)	6643	1256
H	50	18.0	-2.3	90.5	175		
	53	10.7 (0.7)	-2.7 (0.8)	88.7 (3.8)	171.4 (7)	7534	3192
I	65	10	-1	102	*		
	53	14 (0.9)	-3.8 (1.5)	83.9 (4.8)	177.352 (6.1)	7462	1170
J	40	11	-1	93	*		
	53	15.7 (1.1)	-2.8 (1.6)	86.9 (4.8)	179.5 (5)	6815	361

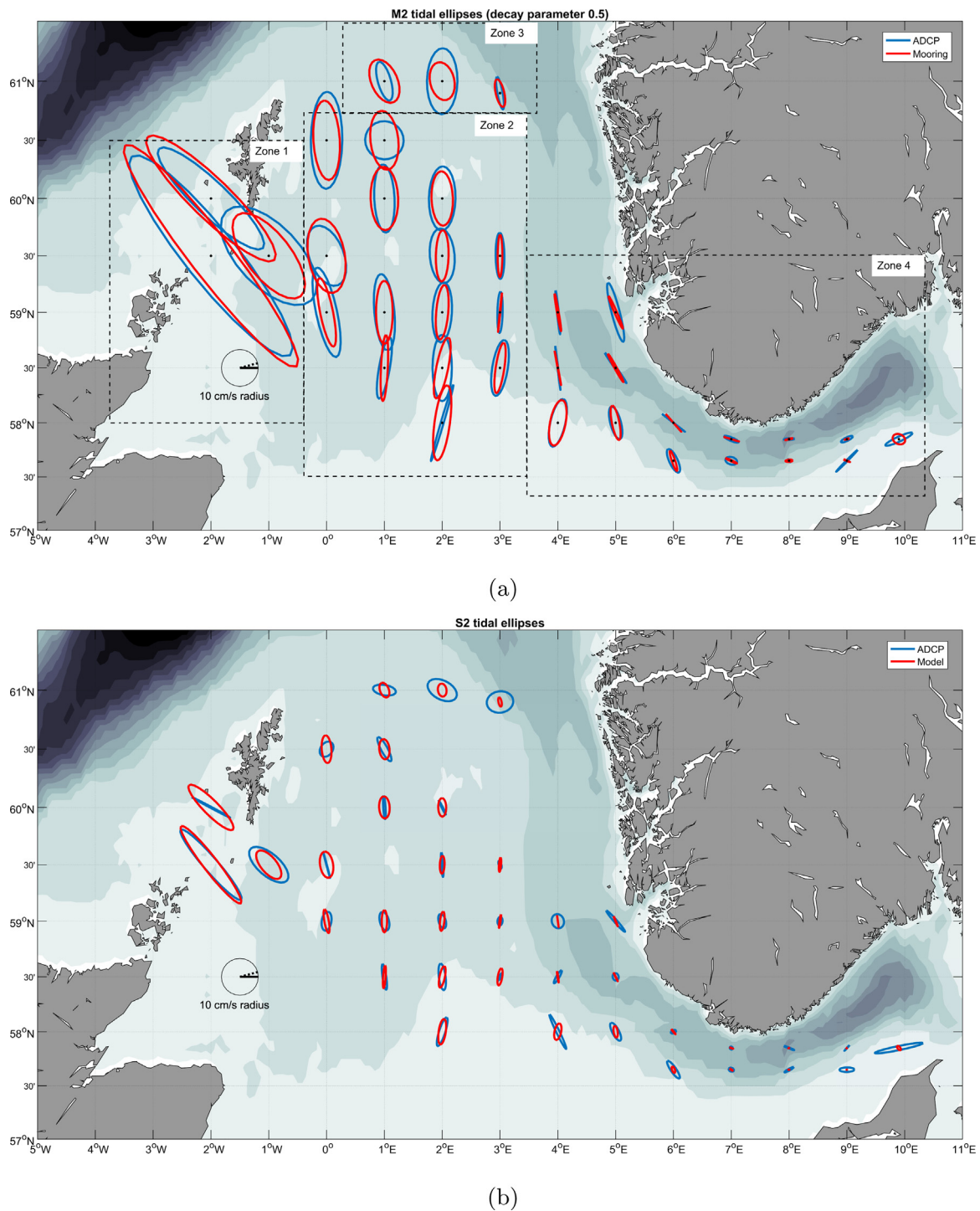


Fig. 6. Tidal ellipses from extracted tidal currents from ADCP measurements in blue compared to tidal ellipses from TPX08-Atlas model. Figs. 6a and 6b show M_2 and S_2 ellipses, respectively. (For interpretation of the references to color in this figure legend, the reader is referred to the web version of this article.)

from the current meter data is 1.8 cm/s. The mean deviations between ADCP and current meter parameters are 3.8 cm/s and 1.4 cm/s, for semi-major and semi-minor axes respectively. These results are similar to the mean deviations of the semi-major and semi-minor axes of the M_2 constituent, but relatively larger given the smaller S_2 current speeds. Ellipse inclination and phase lag do not compare well for the calculated S_2 parameters with the exception of the inclination at moorings A and H where there is a 7.4° and 6.4° deviation, respectively.

Fig. 6a and 6b compare the M_2 and S_2 ellipses from the extracted tides of the ADCP measurements and output from the TPX08-Atlas

regional barotropic tide model. For the M_2 constituent the model output compares well with the ADCP calculated ellipses, e.g., in the Fair Isle Channel, in most of the area of the Norwegian Trench covered by the ADCP, and also on large parts of the plateau west of the Norwegian Trench. In both ADCP and model estimates, the strongest tidal currents for M_2 and S_2 are found in and around the Fair Isle Channel, and the weakest are found in the Norwegian Trench.

Root mean square deviations (RMSD) between the M_2 ellipse parameters calculated from ADCP and those calculated from the TPX08-Atlas model are presented in Table 5. The ellipses were divided

Table 5

Root mean square deviations of M_2 semi-major axis and semi-minor axis (cm/s) along with percentages relative to the average ADCP axes in the respective zones, inclination ($^\circ$), and Phase ($^\circ$ G) when tidal current is directed north, and the average amount of ADCP datapoints used in the calculation of tidal ellipse parameters. Zones 1–4 are shown in Fig. 6a.

	Semi-major	Semi-minor	Inclination RMSD	Phase RMSD	Average datapoints
Zone 1	7 (15.3%)	3.2 (24.5%)	3.3	5.7	6500
Zone 2	2.9 (16.8%)	2.2 (41.5%)	14.6	11.5	6738
Zone 3	4.2 (35.5%)	2.9 (71.3%)	9.2	15.3	477
Zone 4	3 (37.2%)	1.5 (116.7%)	56.1	44.6	12830

into four zones which are shown in Fig. 6a which basically corresponds to a Fair Isle Channel zone, a central plateau zone, a northern zone, and a Norwegian trench zone. Considering the relatively strong M_2 tidal current speeds in zone 1, the RMSD for both semi-major and semi-minor axes are quite small (15.3 % and 24.5 % of the mean values of ADCP axes), and the inclination values agree well between ADCP and model estimates. In zone 2, there is also relatively good agreements with RMSD values of the semi-major and semi-minor axes equal to 16.8 % and 41.5 % of the respective mean ADCP values. The RMSD of the inclination values is relatively low in zones 1–3, at 3.3° , 14.6° and 9.2° . There is less agreement in zone 4, although this is the zone where the ADCP ellipses on average have the most datapoints included in their calculation. Phase RMSD is reported in Table 5 as the RMSD of the phase at the time when the tidal current is directed north. In the case of M_2 ellipses, the direction of the current changes by approximately 29° an hour. A RMSD of 15.3° which is the case in Zone 3, therefore is equivalent to about 30 min difference.

Model and ADCP compare less favorably in the Skagerrak and in the area of zone 3 in Fig. 6a.

4. Discussion

The method used here to extract tidal currents from temporally and spatially variable current measurements allows for determination of tides on a large spatial scale. It has been utilized to detide ADCP data in several studies both in the deep ocean (Childers et al., 2014; Rossby and Flagg, 2012) and in shelf areas and straits (Dunn, 2002; Flagg and Dunn, 2003; Wang et al., 2004) with favourable results. Although current meter data are sparse, we have shown good agreement between ADCP and current meter M_2 ellipses, demonstrating the accuracy of the harmonic analysis of the ADCP data, given that it is limited to areas where ADCP data are relatively densely concentrated. Our estimated parameters of the S_2 tide are also quite accurate with regards to uncertainty, with relatively low standard deviations for all parameters in most areas. On average, standard deviations of the semi-major axes are 11% of the length of the axes. Average standard deviation of the inclination is 12.7° , but in most locations it is well under 10° . The relatively large discrepancies in the comparison of S_2 parameters in Table 4 is likely in part due to the lack of suitable mooring locations to compare with. Phase differences of the S_2 tide between the tides determined from ADCP and from mooring data, are large, meaning that there is a shift between when the two sources yield the strongest S_2 currents. If the phase difference is adjusted to be relative to directionality of the tidal current instead of maximum speed, the deviation decreases, but it is still relatively high in three of four locations, ranging from 12° to 65° . The weaker currents caused by the less predominant tidal constituents are proving harder to determine with the same accuracy. Standard deviation of the K_1 axes, for example, are high relative to the much shorter axes (semi-major axis standard deviation ranges from approximately 10% to approximately 100% of the length of the semi-major axis itself), and standard deviation for the phase calculations which on average over the ten mooring locations averages 88° is not encouraging,

rather it tells us that the method with the current data set does not resolve the weaker components accurately.

The tidal currents calculated from the ADCP current measurements compare well with the general description from previous studies. The M_2 ellipses presented in Fig. 4 are, in the central northern North Sea and in the Norwegian Trench west of Norway, very much meridionally oriented with semi-major axes of around 20 cm/s and 10 cm/s, respectively, as was also found by Klein et al. (1994). Danielssen et al. (1997) and Rodhe (1987) reported very weak tidal currents in the Skagerrak on the order of 1 cm/s. The deeper parts of Skagerrak is indeed where our calculated tidal currents are the weakest and on the scale of a few cm/s, but our calculations also show an increase in current speeds in shallower areas of Skagerrak, on the shelf near the coast of Denmark. Here, both of the dominating semi diurnal tides as well as the O_1 tide produce current speeds of approximately 10 cm/s. The calculated tidal currents in the Fair Isle Channel are the strongest in the study area, and also fit well with the descriptions of conditions in the area from Baxter et al. (2008); Turrell et al. (1990). The tidal currents, driven by the pressure gradient from the difference in surface elevation inside and outside the channel as the tidal wave propagates through it, are intensified here because the flow is constrained by the topography. We see this from both the tidal current speed and the direction of the strongest flow, which is along the channel.

Due to the sparsity of direct current measurements in the northern North Sea, some of the current meter data we have utilized here are located in areas not ideal for comparison with regards to the spatial coverage of the ADCP data. However, they can serve as examples of the sensitivity of the method applied here to extract tides, to data quantity and proximity. The deviation between the inclination angle of the ADCP and current meter ellipses at Mooring B in Fig. 5 and Table 3 can most likely be explained by an effect of the local topography which the ADCP data has not recorded. Many ADCP cruise tracks are found relatively near the location, but most pass several km south of this location. The current meter ellipse at mooring B is oriented parallel to the topography at that location, while the ADCP ellipse is oriented more along the Fair Isle Channel, which suggests that it represents conditions farther south more than at the site of the mooring. Similarly, at mooring I and J, the ADCP ellipses deviate from the narrow current meter ellipses. ADCP data are abundant within a 55.5 km radius of the current meter position, but the quantity is notably reduced when halving the radius. In Fig. 4 the M_2 ellipses located a few tens of km farther south (where ADCP data are more densely concentrated) are much narrower, suggesting that the narrow current meter ellipses at location I and J do indeed describe the actual conditions more accurately. The ADCP data situation is similar at mooring D, but here the ADCP and current meter ellipses compare well. At this location, however, tidal ellipses are more uniform over a larger area, thus the combination of a large decay parameter and an abundance of relatively distant datapoints produce an accurate depiction of the M_2 tidal ellipse here. The same problem of the proximity of the moorings to ADCP datapoints is true at mooring B, and the number of datapoints close to mooring C is perhaps not sufficient.

In this study, we have utilized a relatively large decay parameter in the weighting of the data for the harmonic analysis. Such a large parameter was chosen here in order to determine tidal currents for as large an area as possible, even in the areas that are not the most densely populated with ADCP observations. The choice of decay parameter should be motivated by the abundance of data, and both its temporal and spatial distribution, as well as the physical characteristics of the marine area of interest. With a massive dataset of tightly concentrated data, a smaller decay parameter would be appropriate. In order to resolve a tidal field somewhere one would expect current properties to vary greatly on small spatial scales, e.g. in an area of complex topography, a small decay parameter would be necessary as well. In this study, although we have a large data set, it is widely spread in space as well as in time, making a larger decay parameter useful when analysing

the entire northern North Sea. Experimentation with different decay parameters (see Appendix A) revealed that the sensitivity of the method in this regard is not very high. With values of 0.3, 0.5, and 0.7 degrees the method yielded quite similar results, with 0.5 degrees proving most accurate on average in regards to values of the tidal parameters of the M_2 constituent determined from mooring data, as well as having smaller uncertainties on average. An anisotropic decay parameter was used in weighting function of the harmonic analysis at the location of mooring H in an attempt to reduce the influence of datapoints up on the plateau or farther east in the trench. This improved the similarity between results from ADCP and the observations from the mooring which was located over the western slope of the Norwegian trench, especially in regards to inclination for S_2 , and phase and semi-minor axis for M_2 .

The modeled tide compares well to our harmonic analysis of the ADCP data, the predominant M_2 -constituent especially. With the exception of zone 3 (see Fig. 6a and Table 5) the concentration of ADCP data is dense and numerous, and thus we can expect the accuracy of the tidal currents determined from it to be high. The model output replicates the harmonic analysis quite closely, especially M_2 in zone 1 and 2. The discrepancies in zone 4 presented in Table 5 are large when viewing the percentage error relative to the average value, but Fig. 6a reveals that not all ellipses compare poorly. Rather, the ellipses located on the shelf close to Denmark are the only ones where model and ADCP results do not compare well at all.

The tidal ellipses presented here are located in areas of varying data abundance, and thus of varying accuracy. It is hard to put an exact number on how large a data set is needed for the method to be feasible for a whole area. However, we found that we could reduce the ADCP data set until there were approximately 200 datapoints within 0.25 degrees of latitude of the location of mooring A before the values of the ellipse parameters start to diverge from the values determined from mooring data in this location. The uncertainties at this point, especially of the semi-major and semi-minor axes, grow quite rapidly with the reduction of datapoints as well. Of the ellipses presented in Fig. 4 the three northernmost are located where ADCP datapoints are least numerous, and thus probably the least accurate representations of the actual tidal current. In this area therefore it would be more appropriate to rely on modeled tidal currents, as the model compares well with ADCP results at the remaining ellipse locations over the plateau. Excluding the northernmost area of the plateau, however, the ADCP data are sufficiently abundant to produce relatively precise current estimates for the most dominant tidal constituents (M_2 and S_2) in the study area.

Appendix A. Appendix

A.1. Choice of decay parameter in harmonic analysis of ADCP data

The choice of a decay parameter of 0.5 degrees of latitude was made after experimenting with several different alternatives. In this appendix we present the tidal current ellipse parameter values that result when we apply different decay parameters in the weighting function of the harmonic analysis of the ADCP data. Semi-major and semi-minor axes are presented in Table A1, inclination and phase in Table A2, and standard deviations for all parameters in Table A3. After experimenting with different decay parameters, 0.1, 0.2, 0.3, 0.5, 0.7, and 1 degree, we found that all but the smallest one produced feasible results in at least a few of the locations we looked at (mooring locations from Table 1) with varying degrees of accuracy relative to the parameters calculated from observations from moored instruments. The 3 that performed best with regards to the dominating M_2 tide were 0.3, 0.5, and 0.7. Results from harmonic analysis using these decay parameters are shown in Tables A1, A2 and A3. Which of the decay parameters perform best varies between locations and ellipse parameters. However, averaging over all mooring locations, we find that the 0.5 degree decay parameter results differ least from the mooring results of the semi-major axis and inclination. The standard deviation values (the approach we take to calculate standard deviations is explained in Section 2.2) are also smaller on average for the 0.5 degree decay parameter for semi-major axis values, inclination, and phase. The smaller decay parameter of 0.3 degrees performs well too, in terms of semi-minor axes it is the best performer on average, but in terms of standard deviations, especially for inclination and phase values, it performs worse than 0.5 degrees. 0.7 also yields relatively good results, however, standard deviation values for this decay parameter are also a relatively high on average when compared to the decay parameter of 0.5.

5. Concluding remarks

The accuracy with which the tidal currents can be determined by the harmonic analysis utilized in this study can be expected to improve when applied to larger data sets. While the data set which is utilized here is already quite extensive, separation of constituents will be more successful, and accordingly the reliability of the individual tidal constituent current properties can only increase as monitoring is continued. Especially in areas like the North Sea, where other temporally extensive direct current measurements are rare, continuation of monitoring by instruments on board ships of opportunity will be beneficial to extending our knowledge of the circulation.

With the current data set we have been able to resolve the major semi-diurnal tide in large areas of the northern North Sea. The principal semi-diurnal lunar constituent, M_2 , especially. We are unable to confirm the accuracy of the S_2 results in many areas due to lacking current measurements from moored instruments with which to compare our results, but low standard deviation values for the tidal ellipse parameters are encouraging. The estimated diurnal tides, which have relatively high uncertainties, lead us to conclude that the average half daily tidal cycle is well replicated in our analysis, but we are not able to replicate the modulation of the average tide by lesser constituents with precision.

Acknowledgments

This work was supported by the European Union's Horizon 2020 research and innovation program [grant number 633211]. We are grateful to Dr. Barbara Berx for making available current meter measurements from Marine Scotland Science. These data can be obtained on request, or by visiting the British Oceanographic Data centre online (<http://www.bodc.ac.uk>). We would also like to thank Einar Nygaard at Statoil for providing current meter data from the Norwegian Deepwater Programme. Many thanks to Sandra Fontana and Prof. Thomas Rossby at the University of Rhode Island for the work they have done on the Nuka Arctica project, and for guidance in processing of the data. We are also thankful to Prof. Charles Flagg for making the Norröna data available online (<http://po.msrc.sunysb.edu/Norröna>), and for help with the detiding routine. And thanks to Dr. Ken Drinkwater for proofreading.

Table A1

M_2 tidal current ellipse semi-major and semi-minor axes (Smaj and Smin) calculated from measurements recorded by moored instruments (see mooring information in Table 1, and their location in Fig. 2) and determined from harmonic analysis of ADCP data using three different decay parameters. Values are listed in cm/s.

Decay parameter	Location	Smaj axis (cm/s)			Smin axis (cm/s)		
		Mooring	Adcp	Diff	Mooring	Adcp	Diff
0.5	A	46.4	54.98	8.58	- 11.9	- 11.97	- 0.06
	B	20.4	26.09	5.67	- 11.5	- 13.9	- 2.43
	C	10	13.66	3.65	- 5.8	- 2.11	3.72
	D	14	15.85	1.85	- 5	- 6.69	- 1.69
	E	17	12.95	- 4.05	- 4	- 4.38	- 0.38
	F	19	17.99	- 1.01	- 5	- 4.89	0.11
	G	14	18.08	4.08	- 5	- 5.25	- 0.25
	H	18	11.52	- 6.48	- 2.3	- 3.26	- 0.97
	I	10	14.03	4.03	- 1	- 3.84	- 2.84
	J	11	15.77	4.77	- 1	- 2.81	- 1.81
			Mean diff		4.42	Mean diff	
0.3	A	46.4	57.81	11.4	- 11.9	- 11.81	0.09
	B	20.4	28.97	8.56	- 11.5	- 11.63	- 0.17
	C	10	7.2	- 2.81	- 5.8	- 2.22	3.61
	D	14	15.64	1.64	- 5	- 5.52	- 0.52
	E	17	12.61	- 4.39	- 4	- 3.72	0.28
	F	19	17.29	- 1.71	- 5	- 3.81	1.19
	G	14	17.39	3.39	- 5	- 5.28	- 0.28
	H	18	10.9	- 7.1	- 2.3	- 2.25	0.04
	I	10	13.56	3.56	- 1	- 0.59	0.41
	J	11	15.32	4.32	- 1	0.05	1.05
			Mean diff		4.89	Mean diff	
0.7	A	46.4	53.8	7.39	- 11.9	- 13.78	- 1.87
	B	20.4	26.6	6.19	- 11.5	- 13.41	- 1.94
	C	10	20.3	10.29	- 5.8	- 4.86	0.97
	D	14	16.01	2.01	- 5	- 5.26	- 0.26
	E	17	13.66	- 3.34	- 4	- 3.44	0.56
	F	19	18.16	- 0.84	- 5	- 4.39	0.61
	G	14	18.96	4.96	- 5	- 4.48	0.52
	H	18	11.89	- 6.1	- 2.3	- 1.9	0.39
	I	10	13.85	3.85	- 1	- 1.94	- 0.94
	J	11	15.26	4.26	- 1	- 1.48	- 0.48
			Mean diff		4.92	Mean diff	

Table A2

Same as Table A1 but for inclination and phase. Inclination values are listed in ° counter clockwise from East, and phase values are listed in ° G. Phase difference (diff) is adjusted for the difference in inclination, so it shows angular retardation between ADCP and moored data. A positive difference means that the tidal ellipse determined from ADCP data is leading the ellipse determined from moored measurements.

Decay parameter	Location	Inclination(°)			Phase(°G)		
		Mooring	Adcp	Diff	Mooring	Adcp	Diff
0.5	A	133.3	134.75	1.47	112.2	108.72	2.02
	B	36.1	167.08	130.98	234.2	84.59	18.63
	C	82.8	85.95	3.16	170.4	216.79	- 49.75
	D	97	91.03	- 5.97		166.26	
	E	86	87.1	1.1		161.39	
	F	80	86.09	6.09		164.61	
	G	82	86.47	4.47		162.63	
	H	90.5	89.08	- 1.4	175	165.78	10.62
	I	102	83.85	- 18.15		177.35	
	J	93	86.87	- 6.13		179.52	
			Mean diff		5.33 (excluding B)		
	0.3	A	133.3	132.31	- 0.97	112.2	110.89
B		36.1	173.76	137.66	234.2	80.25	16.29
C		82.8	85.56	2.76	170.4	191.52	- 24.08
D		97	89.11	- 7.89		160.51	
E		86	91.31	5.31		159.82	
F		80	84.81	4.81		164.33	
G		82	88.21	6.22		158.60	
H		90.5	87.3	- 3.18	175	158.82	19.36
I		102	81.64	- 20.36		176.91	
J		93	84.77	- 8.23		184.16	
			Mean diff		6.64 (excluding B)		
0.7		A	133.3	133.06	0.78	112.2	107.81
	B	36.1	154.84	118.74	234.2	98.68	16.78
	C	82.8	107.28	24.49	170.4	217.24	- 71.52
	D	97	94.72	- 2.28		165.98	
	E	86	88.01	2.01		164.08	
	F	80	90.68	10.68		162.60	
	G	82	84.99	2.99		165.14	
	H	90.5	90.84	0.37	175	159.84	14.8
	I	102	82.63	- 19.37		172.04	
	J	93	85.84	- 7.16		174.85	
			Mean diff		7.79 (excluding B)		

Table A3

Standard deviations for each of the four tidal ellipse parameters resulting from use of different decay parameters in the harmonic analysis of the ADCP data. Semi-major and semi-minor axis values (Smaj and Smin) are listed in cm/s. Inclination and phase are listed in °.

Decay parameter	Location	Smaj (cm/s)	Smin (cm/s)	Inclination (°)	Phase (°)
0.5	A	0.61	0.3	0.44	0.6
	B	0.73	0.74	2.83	2.8
	C	1.06	1.41	5.78	4.82
	D	0.48	0.48	2.18	2.47
	E	0.44	0.43	2.35	2.33
	F	0.38	0.3	1.26	1.11
	G	0.44	0.47	1.44	1.38
	H	0.41	0.81	2.91	4.15
	I	0.89	1.55	4.79	6.14
	J	1.08	1.56	4.81	5.02
	Mean		0.652	0.805	2.879
0.3	A	0.74	0.3	0.4	0.53
	B	1.06	1.14	34.81	35.32
	C	0.6	1.11	10.83	11.85
	D	0.44	0.37	1.67	2.12
	E	0.39	0.28	1.42	1.79
	F	0.38	0.28	1.22	1.13
	G	0.42	0.38	1.32	1.44
	H	0.72	0.8	3.82	7.05
	I	1.18	1.7	5.23	10.58
	J	1.34	1.55	4.73	8.4
	Mean		0.727	0.791	6.545
0.7	A	0.58	0.33	0.44	0.59
	B	0.74	0.66	2.37	2.3
	C	2.51	3.4	19.78	18.97
	D	0.45	0.52	2.06	2.22
	E	0.45	0.51	2.6	1.99
	F	0.36	0.32	1.21	1.05
	G	0.44	0.48	1.45	1.22
	H	0.4	0.6	2.61	3.1
	I	0.77	1.11	3.22	4.51
	J	0.87	1.58	3.97	4.3
	Mean		0.757	0.951	3.971

References

- Baxter, J., Boyd, I., Cox, M., Cunningham, L., Holmes, P., Moffat, C. 2008. Scotland's Seas: Towards Understanding their State. Fisheries Research Services, Aberdeen, UK.
- Childers, K.H., Flagg, C.N., Rossby, T., 2014. Direct velocity observations of volume flux between iceland and the shetland islands. *J. Geophys. Res.: Oceans* 119 (9), 5934–5944. <http://dx.doi.org/10.1002/2014JC009946>.
- Danielsen, D.S., Edler, L., Fonselius, S., Hernroth, L., Ostrowski, M., Svendsen, E., Talpsepp, L., 1997. Oceanographic variability in the skagerrak and northern kattegat, may-june 1990. *ICES J. Mar. Sci.: J. Cons.* 54 (5), 753–773. <http://dx.doi.org/10.1006/jmsc.1996.0210>.
- Davies, A.M., Furnes, G.K., 1980. Observed and computed m2 tidal currents in the north sea. *J. Phys. Oceanogr.* 10 (2), 237–257. [http://dx.doi.org/10.1175/1520-0485\(1980\)010<0237:OACMTC>2.0.CO;2](http://dx.doi.org/10.1175/1520-0485(1980)010<0237:OACMTC>2.0.CO;2).
- Dietrich, G., 1950. Die natürlichen regionen der nord- und ostsee auf hydrographischer grundlage. *Kiel. Meeresforsch.* 7, 35–69.
- Dooley, H.D., 1974. Hypotheses concerning the circulation of the northern north sea. *J. Cons.* 36 (1), 54–61. <http://dx.doi.org/10.1093/icesjms/36.1.54>.
- Dunn, M., 2002. A Description of the Barotropic Tide on Georges Bank Based Upon Five years of Shipboard Adcp Observations. (Master's thesis). State University of New York at Stony Brook.
- Egbert, G.D., Erofeeva, S.Y., 2002. Efficient inverse modeling of barotropic ocean tides. *J. Atmos. Ocean. Technol.* 19 (2), 183–204. [http://dx.doi.org/10.1175/1520-0426\(2002\)019<0183:EIMOBO>2.0.CO;2](http://dx.doi.org/10.1175/1520-0426(2002)019<0183:EIMOBO>2.0.CO;2).
- Egbert, G.D., Erofeeva, S.Y., Ray, R.D., 2010. Assimilation of altimetry data for nonlinear shallow-water tides: quarter-diurnal tides of the northwest european shelf. *Cont. Shelf Res.* 30 (6), 668–679. <http://dx.doi.org/10.1016/j.csr.2009.10.011>.
- Flagg, C.N., Dunn, M., 2003. Characterization of the mean and seasonal flow regime on georges bank from shipboard acoustic doppler current profiler data. *J. Geophys. Res.: Oceans* 108 (C11). <http://dx.doi.org/10.1029/2001JC001257>. (8002).
- Foreman, M., 1977. Manual for tidal heights analysis and prediction. *Pac. Mar. Sci. Report.* 77–10.
- Foreman, M., 2004. Manual for tidal currents analysis and prediction. *Pac. Mar. Sci. Report.* 78.
- Furnes, G.K., Hackett, B., Sætre, R., 1986. Retroflexion of atlantic water in the norwegian trench. *Deep Sea Res. Part A. Oceanogr. Res. Pap.* 33 (2), 247–265. [http://dx.doi.org/10.1016/0198-0149\(86\)90121-4](http://dx.doi.org/10.1016/0198-0149(86)90121-4).
- Klein, H., Lange, W., Mittelstaedt, E., 1994. Tidal and residual currents in the northern north sea: observations. *Dtsch. Hydrogr. Z.* 46 (1), 5–27. <http://dx.doi.org/10.1007/BF02225739>.
- Otto, L., Zimmerman, J., Furnes, G., Mork, M., Sætre, R., Becker, G., 1990. Review of the physical oceanography of the north sea. *Neth. J. Sea Res.* 26 (2–4), 161–238. [http://dx.doi.org/10.1016/0077-7579\(90\)90091-T](http://dx.doi.org/10.1016/0077-7579(90)90091-T).
- Pawlowski, R., Beardsley, B., Lentz, S., 2002. Classical tidal harmonic analysis including error estimates in matlab using t_tide. *Comput. Geosci.* 28 (8), 929–937. [http://dx.doi.org/10.1016/S0098-3004\(02\)00013-4](http://dx.doi.org/10.1016/S0098-3004(02)00013-4).
- Rodhe, J., 1987. The large-scale circulation in the skagerrak; interpretation of some observations. *Tellus A* 39 (3).
- Rossby, T., Flagg, C.N., 2012. Direct measurement of volume flux in the faroe-shetland channel and over the iceland-faroe ridge. *Geophys. Res. Lett.* 39 (7). <http://dx.doi.org/10.1029/2012GL051269>.
- Sündermann, J., Pohlmann, T., 2011. A brief analysis of north sea physics. *Oceanologia* 53 (3), 663–689. <http://dx.doi.org/10.5697/oc.53-3.663>.
- Svendsen, E., Sætre, R., Mork, M., 1991. Features of the northern north sea circulation. *Cont. Shelf Res.* 11 (5), 493–508. [http://dx.doi.org/10.1016/0278-4343\(91\)90055-B](http://dx.doi.org/10.1016/0278-4343(91)90055-B).
- Turrell, W., Henderson, E., Slessor, G., 1990. Residual transport within the fair isle current observed during the autumn circulation experiment (ace). *Cont. Shelf Res.* 10 (6), 521–543. [http://dx.doi.org/10.1016/0278-4343\(90\)90080-6](http://dx.doi.org/10.1016/0278-4343(90)90080-6).
- Wang, Y.-H., Chiao, L.-Y., Lwiza, K.M.M., Wang, D.-P., 2004. Analysis of flow at the gate of taiwan strait. *J. Geophys. Res.: Oceans* 109 (C2). <http://dx.doi.org/10.1029/2003JC001937>.